Fundamental Research 5 (2025) 93–102

Contents lists available at ScienceDirect

Fundamental Research

journal homepage: http://www.keaipublishing.com/en/journals/fundamental-research/

Article

Simultaneous recording of neuronal discharge and calcium activity reveals claustrum-cortex neurosynchrony under anesthesia

Penghui Fan[a,b,1], Rujin Zhang[c,1], Guihua Xiao[d,1], Yilin Song[a,b], Chaowei Zhuang[d], Lekang Yuan[e], Fan Mo[a,b], Botao Lu[a,b], Zhaojie Xu[a,b], Yiding Wang[a,b], Jinping Luo[a,b], Mixia Wang[a,b], Weidong Mi[c], Jiangbei Cao[c,*], Qionghai Dai[d,*], Xinxia Cai[a,b,*]

[a] State Key Laboratory of Transducer Technology, Aerospace Information Research Institute, Chinese Academy of Sciences, Beijing 100190, China
[b] University of Chinese Academy of Sciences, Beijing 100049, China
[c] Department of Anesthesiology, The First Medical Center, Chinese PLA General Hospital, Beijing 100853, China
[d] Department of Automation, Tsinghua University, Beijing 100084, China
[e] Tsinghua-Berkeley Shenzhen Institute, Tsinghua University, Shenzhen 518055, China

ARTICLE INFO

Article history:
Received 24 September 2023
Received in revised form 25 December 2023
Accepted 27 December 2023
Available online 5 February 2024

Keywords:
Microelectrode array
Electrophysiology
Neurosynchrony
Anesthesia
Calcium imaging

ABSTRACT

Neural information transmission between deep brain nuclei and the cortex is essential for brain function. Currently, high-resolution simultaneous detection of neural information between the deep brain nuclei and the large-scale cortex still poses challenges. We have developed the microelectrode arrays based on the Micro-Electro-Mechanical System technology, and modified the electrode surface with nanomaterials to improve the electrode performance. This study combined microelectrode arrays and extended-field-of-view microscopy to achieve simultaneous recording of claustrum (CLA) electrophysiology and wide-field cortical calcium imaging at single-cell resolution. This work investigated the synchronous changes of neural information in CLA and cortex of mice during the whole process from wakefulness to anesthesia and then to wakefulness, and summarized the characteristics of the CLA electrophysiology and cortical calcium signaling under different inhalation anesthesia concentrations. We found the synergy between microscopic spike and local field potential of CLA neurons under deep anesthesia, and the law that high inhalation anesthesia concentration enhanced the synchronization between neurons in CLA and cortex. The combination of microelectrode arrays and extended-field-of-view microscopy also gives a new method for synchronous detection of multimodal and multi-brain region neural information.

1. Introduction

High-resolution neural information detection is of great significance for brain science research. The complex interconnectivity of neural circuits within the brain places demands on the simultaneous detection of neural information in multiple brain regions [1–4]. Of these, the synchronous detection of high-resolution neural information between deep brain nuclei and large-scale cortex is particularly important, but currently lacking. The commonly used techniques for detecting brain neural information include Magnetic Resonance Imaging (MRI) [5], Computed Tomography (CT) [6], electrophysiology [7–9], calcium imaging [10,11], etc. Electrophysiological recording has the characteristics of high spatial and temporal resolution, which can realize the recording for rapid single-cell action potential [12]. Microelectrode arrays based on Micro-Electro-Mechanical System (MEMS) technology are considered a promising platform for electrophysiological recording [13], with customizable sites suitable for detecting neural activity in the cortex and deep brain regions [14–16]. Calcium imaging techniques permit the recording of neuronal neural activity over a large range, but limited by optical imaging instruments, the detection range and spatial resolution of calcium imaging are usually mutually constrained [17].

It has been proved that there is a broad projection relationship between the CLA and the cerebral cortex [18,19]. Previous studies have shown that electrical stimulation of the CLA can reversibly disrupt consciousness [20]. This indicates that the CLA is an important brain area related to sleep and consciousness [21]. Anesthesia is a reversible functional depression of the central nervous system caused by drugs or other methods, which is characterized by a temporary state of sensory or consciousness loss. This has sparked our interest in the association between the CLA and cortical neurons during the process of consciousness loss.

Here, we used gradient inhalation anesthesia concentration to simulate the gradual loss of consciousness process, and used simultaneous

* Corresponding authors.
E-mail addresses: caojiangbei@301hospital.com.cn (J. Cao), daiqh@tsinghua.edu.cn (Q. Dai), xxcai@mail.ie.ac.cn (X. Cai).
[1] These authors contributed equally to this work.

https://doi.org/10.1016/j.fmre.2023.12.012

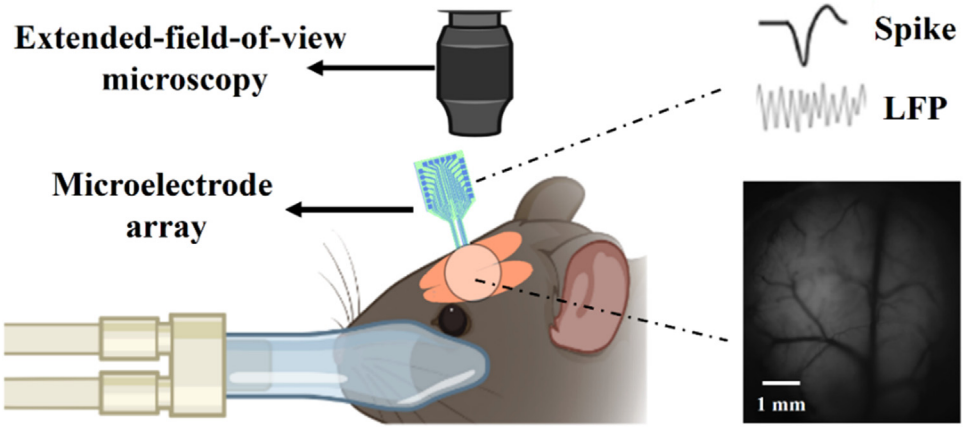

Fig. 1. Experimental schematic diagram. Isoflurane was inhaled into the mouth of mouse through a catheter and the mouse was induced into anesthesia. The CLA of mouse was implanted with microelectrode array to obtain action potential spike and local field potential (LFP). The skull of the mouse head was replaced by a customized chronic cranial window, and the cortical calcium signal was obtained through the extended-field-of-view microscopy. The lower right corner shows the mouse cortex captured under extended-field-of-view microscopy.

electrophysiological recording and calcium imaging to investigate the neural characteristics of CLA and cortical neurons under different inhalation anesthesia concentrations. As shown in Fig. 1, the recording of calcium activity in a single-cell resolution of wide-field cortical neurons is achieved with the help of the real-time brain-wide multi-planar microscopy [22], and the electrophysiology activity of CLA is recorded through the silicon-based microelectrode array.

2. Materials and methods

2.1. Subject

All animal experiments were approved by the Institutional Animal Care and Use Committee at Aerospace Information Research Institute, Chinese Academy of Sciences (AIRCAS), and the Institutional Animal Care and Use Committee at Tsinghua University, Beijing, China.

Four female transgenic mice (Ai148 (TIT2L-GC6f-ICL-tTA2)-D × Rasgrf2-2A-dCre (JAX 030328, JAX 022864)) expressing Gcamp6f protein in the specific layer 2/3 of the cerebral cortex were used in the experiment, all of which were purchased from Laboratory Animal Resource Center, Tsinghua University. The mice are 8 weeks old and weigh 20–25 g. All animals are housed in the animal room with a temperature of 20–22 ˚C and relative humidity of 50% (± 3%), in which 12 h of light and 12 h of darkness cycle alternately. All animals have free access to food and water. We try our best to reduce the number of experimental animals and reduce their pain.

We injected trimethoprim (TMP, 0.25 mg/g, Sigma) intraperitoneally into P36 mice for two consecutive days to induce Cre expression, thus making the vertebral neurons of mice cortex layer 2/3 express green fluorescent protein.

2.2. Microelectrode array manufacturing and performance characterization

CLA is a deep and small brain region in rodents, which requires high accuracy of electrode positioning. Compared to flexible electrodes, rigid silicon-based microelectrode arrays are easy to implant and have high positioning accuracy. Therefore, we used self-made silicon-based microelectrode arrays as electrophysiological recording devices. The silicon-based microelectrode arrays were designed as two needle-like shanks with 16 detection sites arranged at the tip. The electrode length is 6 mm, and width is 500 μm. The diameter of electrode detection site is 15 μm. The device is of a sandwich structure, and the thickness of underlying silicon is 25 μm. The thickness of the middle conductive layer Ti/Pt is 30 nm and 250 nm respectively, and the upper insulating layer adopts the double insulating layer SiO_2/Si_3N_4, with the thickness of 300 nm and 500 nm.

The microelectrode arrays were developed using MEMS technology (Fig. S1). The electrode fabrication process can be summarized as three steps. First, the first photolithography is performed on the thermally oxidized SOI (Silicon on Insulator) wafer, and the conductive layer (Ti/Pt) is formed after sputtering and lift-off. Then, deposition of the insulating layer (SiO_2/Si_3N_4) is followed by plasma etching to expose the detection sites and pads. Finally, the photoresist mask is formed by the third photolithography, the electrode profile is formed by deep etching, and the back wet etching is used to release the electrodes [23,24]. The device after electrical encapsulation is shown in Fig. 2a.

The electrodes were modified with a combination of platinum black nanoparticles and conductive polymers PEDOT (PtNPs/PEDOT:PSS) [23]. Fig. 2b shows the microscope morphology of the electrodes, which are covered with a dense nanolayer. Fig. 2c-d shows the impedance spectrum and Nyquist spectrum of the modified electrode. The impedance of the modified electrode is 29.8 ± 3.4 kΩ, and the phase delay is −16.2˚ ± 0.85˚, demonstrating the excellent electrical performance of the electrode. Fig. 2d shows the electrochemical characteristics of the electrode, indicating that the electrode can approximate an equivalent circuit model where charge transfer control and diffusion processes coexist. Fig. 2e shows the in vivo electrophysiology recording high-frequency signals, indicating that the electrode has excellent performance. The PtNPs/PEDOT:PSS modified electrode can work normally in vivo for more than 100 days. Fig. S2 shows the original neural signals and typical action potential waveforms recorded at 7 days, 21 days, 100 days and 140 days after the electrode was implanted into the brain. From the figure, it can be seen that with the increase of implantation time, the electrode performance (signal-to-noise ratio) decreases. This may be due to the fact that as the implantation time increases, the fibrous encapsulation of the brain causes electrode performance degradation. While in this short-term anesthesia study, since each experiment only takes about 30 min, we believe that the degradation of electrode performance was negligible and would not affect the experimental results.

2.3. Electrode implantation and chronic cranial window replacement surgery

One week after the TMP injection, we performed electrode implantation and chronic cranial window replacement surgery on mice. We have practiced for a long time to ensure that we can successfully complete the electrode implantation and cranial window replacement surgery.

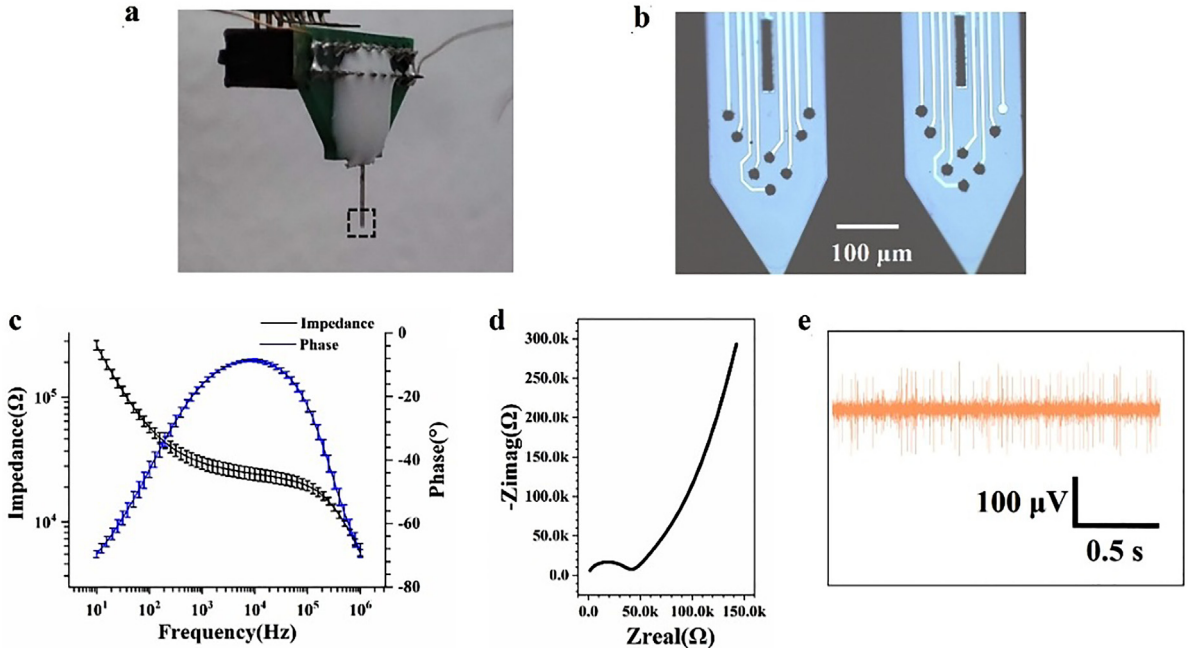

Fig. 2. Physical view of microelectronic array and characteristic of electrode performance. (a) Physical electrode diagram; (b) Microscopic images of modified electrode detection sites, which is an enlarged view of the dashed rectangle in Fig. 1a; (c) Impedance spectroscopy of modified electrode (n = 9 electrode sites), data are means ± SE; (d) The Nyquist diagram of the modified electrode; (e) High frequency electrophysiological signals detected by modified electrodes.

We also pay great attention to disinfection during surgery to avoid the occurrence of infection. The mouse under surgery was placed in the induction box (Isoflurane concentration 3%, oxygen flow 1 L/min) of the anesthesia machine (RWD Life Science Technology Co., Ltd., Shenzhen). After the righting reflex of the mice disappeared, they were transferred to the brain stereotaxic frame (RWD Life Science Technology Co., Ltd., Shenzhen), and the anesthesia was maintained with an isoflurane concentration of 1%-1.5% and an oxygen flow of 0.5 L/min. A heating pad with a temperature controlled at 36.5 ˚C was placed in the abdomen of the mouse to maintain the body temperature. Erythromycin eye ointment (Nanjing Baijingyu Pharmaceutical Co., Ltd., Nanjing) was used to cover the eyes of the mouse to avoid damage to the eyes by the operating lamp. After the hair of the mouse was shaved, the skin on the mouse head was disinfected with iodophor (Shandong Lierkang Medical Technology Co., Ltd., Dezhou), and cut off, and the connective tissue on the surface of the skull was removed. The skull was wiped with a cotton swab to expose the frontal and lambda points of the mouse, and the head was leveled according to these two points.

The bregma point was chosen as the center point to determine the electrode implantation position (AP: −0.15 mm, ML: 3.60 mm). A 1 mm × 1 mm hole was drilled in the skull as the electrode implantation window. The MEA was fixed on the holder of the stereotaxic frame and connected to the electrophysiological acquisition system (Plexon Neural Recording Data Acquisition System, Plexon Inc, Dallas, Texas). The MEA was slowly implanted and the electrophysiological signal was monitored in real time to determine the optimal electrode implantation position within 4.4 ± 0.1 mm depth range. Fig. S3a shows the physical image of electrode implantation surgery. The MEA was fixed on the skull with tissue glue (3 M Vetbond). After waiting for 5 min to make the glue completely dry, the MEA was re-fixed with dental cement. In the implantation operation, the electrode implantation position and surgical trauma have a great influence on the recording of neural activity. In order to make the electrode record more cells, we kept the signal recording during the electrode implantation process. In this process, the operating table is shielded to prevent the electromagnetic interference and obtain the neural signal (Fig. S3b). In order to avoid excessive surgical trauma caused by electrode implantation, we tried to reduce the size of the skull window for the electrode, and used physiological saline to keep the mouse head moist. In addition, we have prepared enough hemostatic sponges to stop bleeding in time.

To realize the synchronous acquisition of the whole cortex calcium imaging and CLA electrical signals of mice, we replaced part of the mouse skull with the chronic optical window. During the operation, an about 7 mm diameter round skull with the bregma point as the center was removed to expose the mouse brain tissue. In order to avoid mutual influence between the optical window and the electrode, the chronic optical window is isolated from the electrode implantation window by a narrow skull. After covering the exposed brain tissue with a transparent cover glass which was pre-polished to better fit the exposed brain tissue, a chronic optical window was formed for whole-cortical calcium imaging. 3 M tissue glue with good biocompatibility was used to bond the cover glass with the skull. After the glue is completely solidified, a custom-made semi-circular aluminum head post was fixed to the skull of the mouse with dental cement to assist in the fixation of the mouse's head in subsequent experiments. The photos of electrode implantation and surgery completion are shown in Fig. S3c.

After the operation, the mice were kept in a single cage for 12 h and were given sufficient water and food, as well as a 36.5 ˚C thermostatic heating pad. On the 7th day after the operation, we fixed the mice under a wide-field microscope in a dark environment and put a mask on the face of the mice to give 0.5 L/min flow of oxygen to carry out adaptive training for the mice. After a few days of acclimatization, the experiments began.

2.4. Anesthesia paradigm

The mice were placed in a dark environment for half an hour before the formal experiment began. 0–3 min after the experiment, the mice only inhaled oxygen at a flow rate of 0.5 L/min. The data collected during this period is set as the baseline. 0.5% isoflurane was applied in the 3rd minute and lasted for 2 min. The concentration of isoflurane increased to 0.8% in the 5th minute, 1.2% in the 7th minute, 1.6% in the 9th minute, and 2.0% in the 11th minute. The concentration of isoflurane decreased to 1.6% at the 14th minute, 1.2% at the 16th

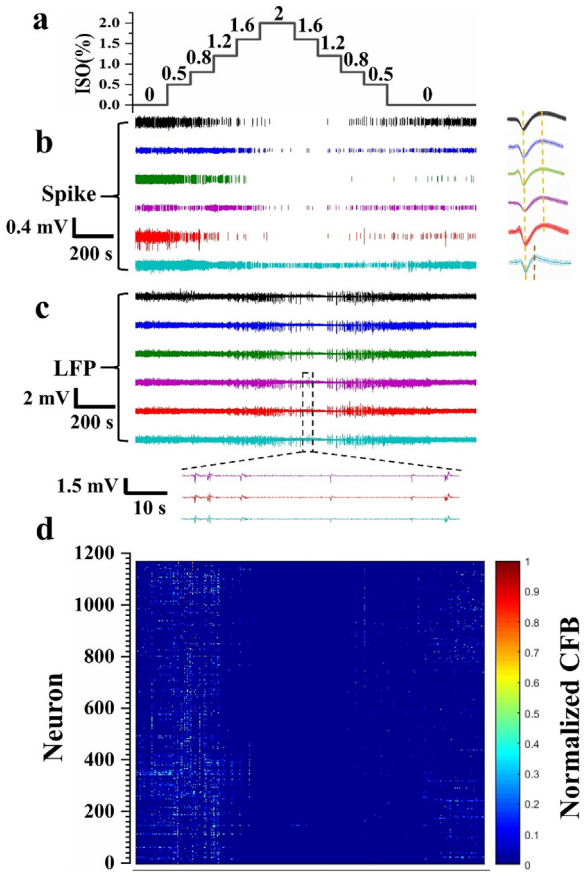

Fig. 3. Synchronous changes of CLA electrophysiology and cortical Calcium signaling. (a) Inhalation anesthesia concentration paradigm; (b) Typical spike sequence of 6 channels; (c) Typical LFP of 6 channels, The dotted box is a local enlarged picture; (d) Calcium signal hot spots of 1168 neurons in the cortex.

minute, 0.8% at the 18th minute, 0.5% at the 20th minute, and closed at the 22nd minute (Fig. 3a). In the above process, the wide-field calcium imaging signal and the electrophysiological signal were collected simultaneously (Fig. 3b-d).

2.5. Wide-field calcium imaging and CLA electrophysiological signal acquisition

We use the method of fixing the mouse head for synchronous recording of electrophysiology and calcium imaging, which can avoid movement interference (Fig. S3d). The calcium signal of cortical neurons is collected through the self-developed fluorescence microscope system. The field of view of the system is about 6 mm, and the corresponding size of each pixel of sCMOS on the plane is 3.25 μm. The acquisition software is HCImage Live (Hamamatsu), and the exposure time is 100 ms. The shooting frequency is 10 Hz.

The electrophysiological signal is obtained by connecting the microelectrode array to the Plexon electrophysiological system. The sampling rate is 40 kHz. The action potential spikes were obtained by applying high-pass filtering at 250 Hz, and the local field potential (LFP) was obtained by applying low-pass filtering at 250 Hz. Electrophysiology recording is highly susceptible to interference, which comes from optical instruments and the surrounding environment. In the experiment, we adopted the method of connecting the optical instrument and the experimental platform with the ground of the electrophysiological instrument, and using the shielding cloth to wrap the experimental platform as much as possible. Time synchronization is achieved between the calcium imaging system and the electrophysiological system through a time labeling module. Fig. S3d shows the mouse during the experiment.

2.6. Data processing and analysis

Electrophysiological signals: The high-frequency signal was denoised by Offline Sorter software, and the further analysis of the electrophysiological signal is completed by NeuroExplorer software. The LFP power of different frequency bands is calculated using Python programming algorithms. The power spectral density of LFP and spike is calculated through the “Power Spectral Densities” function in NeuroExplorer. LFP correlation is defined as the Pearson correlation coefficient between the current channel LFP and the average LFP of other channels. The burst suppression rate is defined as the ratio of the duration of the suppression wave to the total duration, where the suppression wave must have a waveform amplitude less than the threshold and last for 100 ms [25], and the threshold is defined as the minimum amplitude that does not meet the requirements for the occurrence of the suppression wave during the no anesthesia phase.

Cortical neuron calcium signal: By adopting deep-learning-based wide-field neuron finder (DeepWonder) [26], the average calcium fluorescence brightness (CFB) of neurons in all images is extracted to obtain information on the changes in the neuron calcium signal over time. Cortical neuronal synchronicity is defined as the Pearson correlation coefficient between the current neuronal calcium signal and the average value of other neuronal calcium signals.

To study the effects of different inhalation anesthesia concentrations on neural activity, the experiment was divided into different anesthesia stages based on the inhalation anesthesia concentration. Due to the longer duration of the stage after turning off anesthesia, in order to ensure consistency in data analysis and statistical standards at various anesthesia concentrations, the entire stage after turning off anesthesia is further divided into three small stages. The entire experiment is divided into the following stages: 0%, 0.5%, 0.8%, 1.2%, 1.6%, 2%, 1.6%, 1.2%, 0.8%, 0.5%, 0%, 0%, and 0%. The data selected for each stage during statistical analysis is of equal duration.

3. Result

3.1. Simultaneous detection of electrophysiology and calcium imaging under different inhalation anesthetic concentrations

The anesthesia paradigm can refer to methods and Fig. 3a. The typical dynamic changes of spikes, LFP in CLA, and calcium signal of cortical neurons under different inhalation anesthetic concentrations are shown in Fig. 3. Fig. 3b shows the action potential raster plot detected by six different channels, which are displayed using different color. The figure shows that as the inhalation anesthesia concentration increases, the frequency of spikes firing gradually decreases until it disappears. Conversely, when the anesthesia concentration decreases, the spike frequency gradually increases (Fig. 3b). In the experiment, we also detected neurons that continued to discharge under high inhalation anesthesia, such as the sixth neuron in Fig. 3b (shown in cyan). Comparing the mean spike waveforms of neurons, we found that the sixth neuron had a smaller pulse width and may belong to a different type from other neurons. Fig. S4 shows the interspike interval histogram of spikes in Fig. 3b, which confirm that this signal is meaningful. In terms of LFP, when the inhalation anesthetic concentration gradually increases to 1.2%, the amplitude of LFP will increase significantly. As the inhalation anesthetic concentration continues to increase, there will be obvious burst suppression waves (local enlarged image of LFP), which was defined as the pattern consisting of a continuous alternation between high-voltage slow waves (occasionally sharp waves) and depressed (or suppressed) electrographic activity [27]. After that, with the decrease of inhalation anesthesia concentration, the LFP waveform gradually recovered to the normal state (Fig. 3c). In terms of calcium fluorescence brightness (CFB)

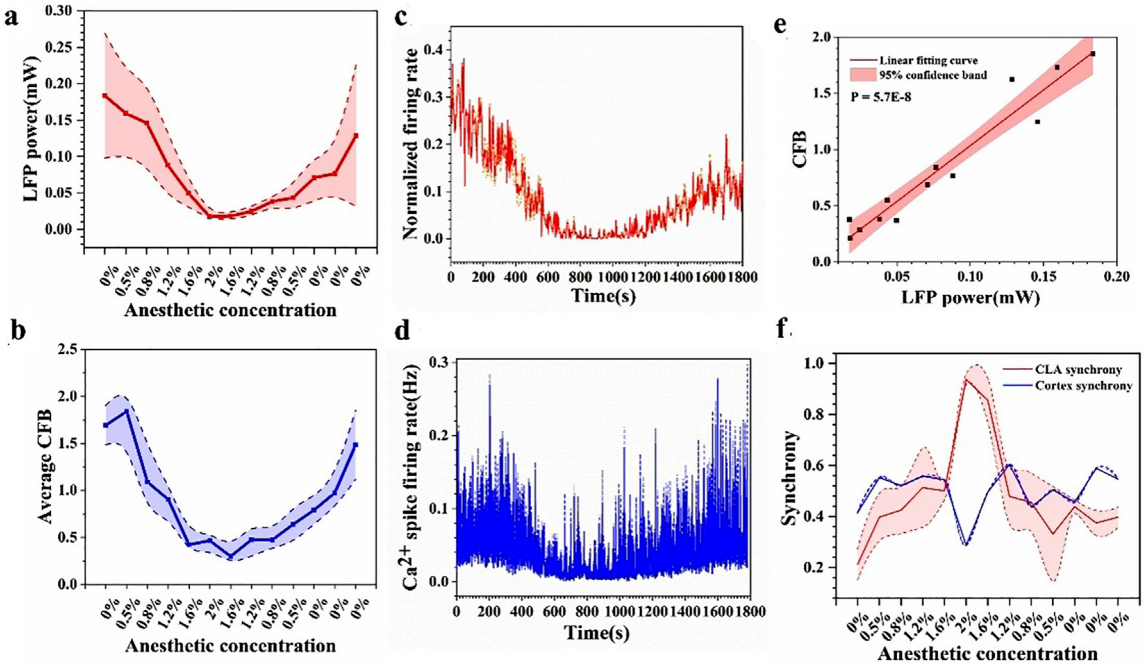

Fig. 4. Electrophysiological and cortical calcium signaling indices at different inhalation anesthesia concentrations. (a) LFP power in gamma frequency band at different inhalation anesthetic concentrations (n = 3 mice); (b) Average calcium fluorescence brightness (CFB) under different inhalation anesthesia concentrations (n = 4 mice); (c) Normalized spike firing rate with the bin of 5 s. (n = 3 mice); (d) Ca^{2+} spike firing rate under different inhalation anesthesia concentrations (n = 4 mice); (e) Fitting curve of LFP power in CLA and cortical neuron calcium fluorescence brightness (CFB); (f) CLA neurons synchrony and cortex neurons synchrony under different inhalation anesthesia concentrations (n = 3 mice). Data are means ± SE.

of cortical neurons, it can be seen that some cortical neurons are significantly activated at low inhalation anesthetic concentrations (0.5% and 0.8%), which may be due to the stimulation of the cerebral cortex caused by low inhalation anesthesia concentration. And with the increase of inhalation anesthesia concentration, the calcium signal of cortical neurons weakened and the neurons were gradually inhibited (Fig. 3d). Through simultaneous detection of electrophysiology and calcium imaging, we observed the dynamic response of CLA neurons and cortical neurons with the change of inhalation anesthesia concentration. When the concentration of inhalation anesthesia was reduced to 1.6%, the degree of neuron inhibition is the largest, which can be attributed to the cumulative effect of anesthesia.

Fig. S5 shows the synchronous change of spike firing rate and LFP power spectrum during the experiment. It can be seen from the figure that with the change of inhalation anesthesia concentration, the spike changes synchronously with the LFP. After that, the power spectral density of low-frequency (0–30 Hz) LFP was analyzed. As shown in Fig. S6, the LFP power in 1–4 Hz (delta band) increased at low inhalation anesthesia concentration (0.8%, 1.2%, and 1.6%), which is also reflected in Fig. S5. When the inhalation anesthesia concentration reached 2%, the overall frequency band power decreased significantly. When the concentration of inhalation anesthesia decreased to 0.8%, the power spectral density gradually recovered.

3.2. Characteristics of CLA electrophysiology and cortical calcium signal under different inhalation anesthesia concentrations

We calculated some indicators of CLA electrophysiology and cortical neuronal calcium signals under different inhalation anesthesia concentrations, as shown in Fig. 4. Fig. 4a shows the LFP power change in the gamma band (50-100 Hz) under different inhalation anesthetic concentrations, which is considered as an indicator to evaluate the degree of anesthesia. It can be seen from Fig. 4a that the LFP power in the gamma band decreases progressively as the inhalation anesthesia concentration increases, and then with the decrease of inhalation anesthetic concentration, the LFP power in the gamma band increases, indicating that the degree of anesthesia in mice is also changing with the change of inhalation anesthetic concentration. Fig. 4b shows the changes in the average calcium fluorescence brightness of cortical neurons under different inhalation anesthesia concentrations. As can be seen from Fig. 4b that the CFB increases at 0.5% inhalation anesthesia concentration, and then gradually decreases with the increase of inhalation anesthesia concentration, reaching the lowest level at 1.6% inhalation anesthesia concentration. Fig. 4c shows the change of the average spike firing rate (bin of 5 s) of neurons in CLA from the beginning to the end of the experiment. The changing trend of spike firing rate is similar to that of LFP power. And the spike firing rate decreases to the lowest during the period of high inhalation anesthesia concentration. Similarly, we calculated the calcium spike firing rate of cortical neurons. It increased at 0.5% inhalation anesthesia concentration (180 s–300 s), and then gradually decreased with the increase of inhalation anesthesia concentration. The overall trend is consistent with the firing rate of CLA neurons (Fig. 4d). These all reflect the consistency of the effects of anesthesia on CLA and cortical neurons. By fitting the LFP power in CLA and cortical neuron calcium fluorescence brightness under different inhalation anesthesia concentrations (Fig. 4e), it was found that there is a strong correlation between the two, with a linear fitting coefficient of 0.94. Then this study analyzed the correlation between LFPs and found that LFP synchronization was higher at high inhalation anesthesia concentrations, while for cortical neurons, the opposite was true. At the highest inhalation anesthesia concentration, the correlation between cortical neurons was the lowest (Fig. 4f).

In addition, we also defined the ratio of LFP power in the delta frequency band (1–4 Hz) to the gamma frequency band. This indicator sharply increases when the degree of inhalation anesthesia is high, indicating that as the degree of inhalation anesthesia increases (Fig. 5a), there is less reduction of LFP power in the delta band compared to the gamma band. For the single neuron action potential, this study calculated and counted the variance of the firing sequence of each neuron over time. It can be seen that the variance of the firing sequence of

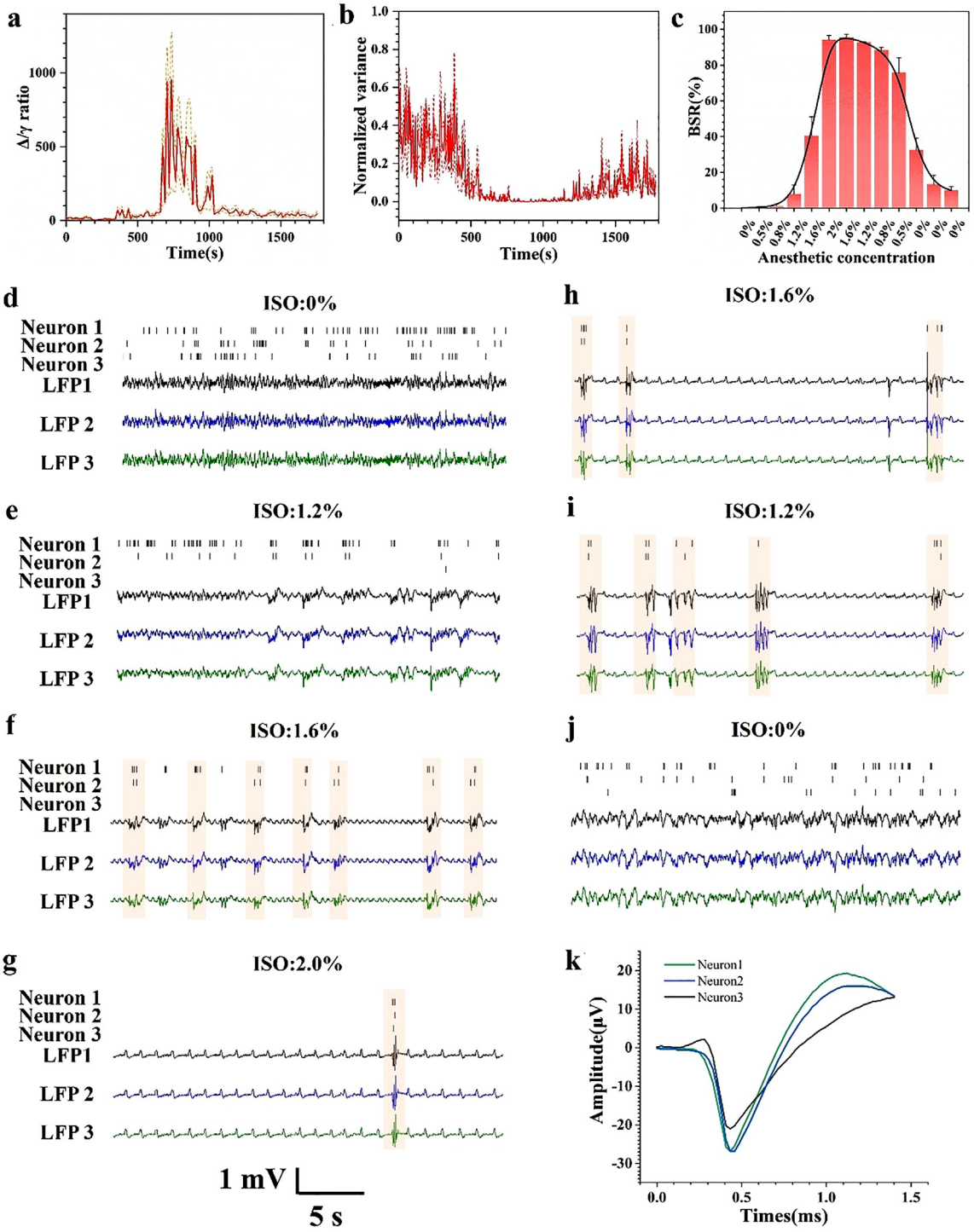

Fig. 5. CLA electrophysiological characteristics under different inhalation anesthesia concentrations. (a) The ratio of delta-band LFP power to gamma-band LFP power ($n = 3$ mice); (b) Variance of spike firing rate ($n = 3$ mice); (c) Burst suppression rate at different inhalation anesthesia concentrations ($n = 3$ mice); (d)-(j): Spike sequences and LFP waveforms at different inhalation anesthetic concentrations, the pink shadow indicates that the spike and LFP bursts appear at the same time. (k) Average Action potential waveform of neurons 1–3. Data are means ± SE for (a)-(c).

each neuron decreases with the increase of inhalation anesthesia concentration, indicating that the activity of each neuron tends to be more consistent with the deepening of anesthesia (Fig. 5b). Burst suppression rate (BSR) is a classic index to measure the degree of anesthesia, which is defined as the proportion of the duration of suppression wave to the total duration [27,28]. We calculated the BSR of CLA under different anesthetic concentrations (Fig. 5c). At the stage of gradual increase of inhalation anesthetic concentration, the BSR increased rapidly, while at the stage of gradual decrease of inhalation anesthetic concentration, the BSR decreased slowly, which indicates that entering the anesthetic state is faster than recovering from anesthesia. The generation of burst suppression is due to the hyperpolarization of individual neurons during deep anesthesia. With the advantage of MEAs, we also detected the neurons that continue to discharge during deep anesthesia, and the time of spikes firing corresponds to the burst period of LFP. Fig. 5d-j shows the action potential spikes of 3 neurons and LFP of 3 channels under

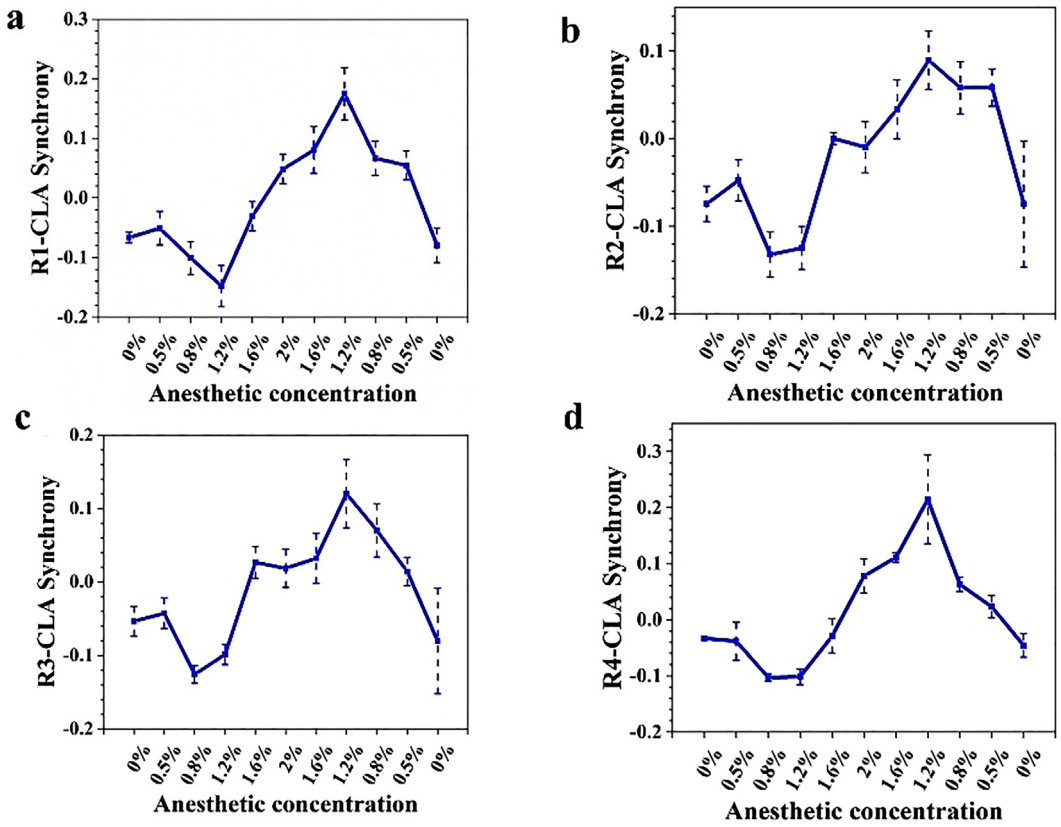

Fig. 6. Synchrony of CLA neurons with cortical neurons at different concentrations of inhalation anesthesia. (a): Synchrony between CLA neurons and motor cortex neurons; (b) Synchrony between CLA neurons and somatosensory cortical neurons; (c) Synchrony between CLA neurons and visual cortical neurons; (d) Synchronization of CLA neurons with retrosplenial cortical neurons. $n = 3$ mice. Data are means ± SE.

different anesthesia concentrations. It can be seen that spike firing become sparse under deep anesthesia, and the spike firing of Neuron 1 and Neuron 2 corresponded to the burst period of LFP. This may reflect the synergistic effect between microscopic spikes and LFP. Then we compared the average action potential waveform of these three neurons, as shown in Fig. 5k. From Fig. 5k, it can be seen that the waveforms of neurons 1 and 2 are relatively similar, and they are quite different from the waveforms of neurons 3. We speculate that specific neurons are coordinating neural information transmission under deep anesthesia. The amplitude of the neuron action potential waveform shown in Fig. 5k is lower than that in Fig. 2b. This may be due to the different types of neurons recorded by the two, or may be due to the obvious difference in the distance between the recorded neurons and the electrodes.

Fig. S7 shows the power spectral density of spike and LFP. It can be seen from the diagram that the spike power density decreased after anesthesia, which was due to the decrease of spike firing rate after anesthesia. The low-frequency LFP power density increased after anesthesia, which was consistent with the results of Fig. S3 and S4. More importantly, we found that the spike and LFP power density spectra were more consistent after anesthesia, and both have characteristic peaks in the delta frequency band. This also reflects that anesthesia enhances the synergy between spikes and LFP.

Finally, we studied the effects of different inhalation anesthetic concentrations on the spike waveform. Because most of the neurons did not discharge when the inhalation anesthetic concentration was 2% and 1.6%, the whole stage was divided into pre (before anesthesia), 0.5%–0.8%, 1.2%–1.2% (including 1.2%, 1.6%, 2%, 1.6%, and 1.2% inhalation anesthesia concentration), 0.8%–0.5%, and post (after stopping anesthesia). We calculated the average spike amplitudes of 28 neurons at different inhalation anesthesia concentrations, normalized it for one-way repeated measures ANOVA analysis. We found that the amplitude of spike waveform changed regularly, that is, as the whole experiment progressed, the amplitude of spike waveform gradually decreased (Fig. S8a). This may be because the mice did not fully recover from anesthesia until the experiment was stopped.

3.3. Calcium signal response of cortical neurons under different inhalation anesthetic concentrations

This study attempts to classify cortical neurons based on their response to inhalation anesthesia concentration, i.e., they are classified as neurons that are suppressed after a specific inhalation anesthesia concentration. For example, Type05 indicates that the average calcium fluorescence brightness of this type of neurons begins to decrease during the 0.5% inhalation anesthesia concentration stage, that is, the calcium fluorescence brightness of this type of neurons during the non-anesthesia stage is the highest value throughout the entire experimental process. Type08 indicates that the average calcium fluorescence brightness of these neurons begins to decrease during 0.8% inhalation anesthesia concentration, that is, the calcium fluorescence brightness of these neurons during the 0.5% anesthesia concentration stage is the highest value throughout the entire experimental process. This study found that neurons suppressed by inhalation anesthesia concentration of 0.5%, 0.8%, and 1.2% accounted for 31.06%, 31.55%, and 19.91%, respectively (Fig. S9a). The average calcium fluorescence brightness (CFB) of these types of neurons was calculated in this study. Fig. S9b shows the temporal variation of the average CFB of the five main types of neurons. From the graph, it can be seen that the stages with the highest calcium signal brightness of these 5 types of neurons shift rightward along the time axis.

In this study, the cortical images were partitioned according to the standard brain atlas [29]. As shown in Fig. S10a, the cortex was divided

into 4 brain regions, namely 1-motor cortex, 2-somatosensory cortex, 3-visual cortex, and 4-retrosplenial cortex. Fig. S10b shows the distribution of neurons detected in these 4 brain regions, which shows that wide-field imaging has single-cell resolution. Subsequently, this study statistically analyzed the average CFB values of four cortical region neurons under various inhalation anesthesia concentrations, as shown in Fig. S11. We found that except for the motor cortex, the average CFB of neurons in other brain regions at 0.5% inhalation anesthesia concentration is higher than that before anesthesia. Fig. S12 shows the correlation of calcium signals in different brain regions. The correlation of neurons in the motor cortex, sensory cortex, and visual cortex is low under high inhalation anesthesia concentration, while the correlation of neurons in the retrosplenial cortex is higher under high inhalation anesthesia concentration. It is evident here that there are large differences in neuronal responses in different brain regions at different inhalation anesthesia concentrations, which may be related to brain region function.

3.4. Analysis of synchrony between deep brain area CLA neurons and cortical neurons under different inhalation anesthesia concentrations

We analyzed the synchrony between cortical neurons and CLA neurons by calculating the correlation coefficient between calcium signals of neurons in different cortical regions and LFP in CLA under different inhalation anesthesia concentrations, as shown in Fig. 6. As can be seen from the graph, the synchrony between cortical neurons and CLA neurons decreased at the beginning of the experiment during the low inhalation anesthesia stage, which may be due to the difference in response to anesthesia between cortical neurons and deep brain area CLA neurons at low inhalation anesthesia concentrations. And then the synchrony gradually increased as the anesthesia level increased, reaching a maximum at the inhalation anesthesia concentration reduced to 1.2%. We noticed that the synchrony decreased again when the concentration was 2% in the somatosensory area and visual areas. Overall, the synchrony trend between the neurons in the four cortical regions and CLA neurons is consistent, and deepening anesthesia will enhance the synchrony between the cortex and CLA neurons. This trend of synchronicity is also echoed by the electrophysiological and calcium signals shown in Fig. 3. The decrease of synchronization under low inhalation anesthesia concentration may be related to the response of cortical neurons under low inhalation anesthesia concentration, while the increase of synchronization under high inhalation anesthesia concentration may be related to the decrease of CLA and neural activity of cortical neurons under high inhalation anesthesia concentration.

After that, we statistically analyzed the correlation between the neurons in the four cortex regions and the neurons in CLA. As shown in Fig. S13, the correlation between the motor cortex and CLA is the highest.

4. Discussion

The integration of electrophysiology, which can analyze submillisecond neural activity, and optical imaging has already been carried out in many studies. Yi Qiang et al. developed a transparent microelectrode array, which was combined with two-photon imaging to achieve synchronous recording of electrophysiology and calcium imaging of the visual cortex [30]. Both electrophysiological and optical calcium imaging are applied to the same brain area. Kerekes et al. combined linear multielectrode array, patch clamp, and two-photon imaging techniques to synchronously record the spontaneous synchronous population activity of human neocortical slices [31]. This study achieved intracellular and extracellular electrophysiological recording and calcium imaging recording of the brain slice. This is an application of in vitro recording. With the development of protein molecular technology, the researchers developed a voltage indicator (Kv-ArcLight-ST) that can co-express with calcium indicators in cells [32], achieving synchronous recording of cellular calcium and voltage signals. The authors combined this imaging technique with LFP recording to study the neural activity of the visual cortex during seizures. But relatively few means of ensuring high-resolution recording of cortical neural information over a large area. Here we have combined microelectrode arrays and extended-field-of-view microscopy to achieve simultaneous recording of neural information at single-cell resolution from CLA electrophysiology and wide-field cortical calcium signals. This protocol allows for the simultaneous acquisition of action potentials, LFP information in deep brain nuclei and calcium activities of large-scale cortex neurons. We took full advantage of this combination of electrophysiological and calcium imaging to compare the neural characteristics of CLA and cortex under different inhalation anesthesia concentrations. Importantly, we investigated the synchronization of the neurons and found that anesthesia enhanced the synchronization of neural activity in CLA and cortex.

There is a wide connection between the CLA and the cortex, and the stimulus response relationship between the CLA and the cortex has been reported [33,34]. At present, there is relatively little research on the synchronous recording of neural activity in CLA and multicortical brain regions. The study of the relationship between the CLA and the cortex is mainly through single brain region recording, regulation and anatomy. In this study, we proposed the method for simultaneous detection of deep brain electrophysiology and cortical calcium imaging by combining microelectrode array with wide-field microscopy. Using this method, we studied the synchronous neural activity changes in the CLA and cortex during the whole anesthesia process. Since the neural activity of the CLA and cortex can be recorded at the same time, we focus on the synchronization between the two, which is different from the previous studies. With the advantage of simultaneous detection of neural information from the CLA and the cortex, this study compared the characteristics of neural information in CLA and cortex and found that their neural activity trends were consistent, both decreasing with increasing inhalation anesthesia concentration. The difference is that low inhalation anesthesia concentration can stimulate cortical neurons and have a certain activation effect on cortical neuronal activities, while it has almost no effect on the CLA neurons (Fig. 4a-b). This is consistent with previous reports, in which the amplitude of EEG signals increased under low anesthesia concentration, and was completely suppressed as the anesthesia concentration deepened [27]. In addition, there is also a significant difference in neuronal synchronicity between the two. The correlation of neural activity in CLA increases with the increase of inhalation anesthesia concentration, while the correlation of neural activity in the cortex decreases with the increase of inhalation anesthesia concentration. This may be due to the large area of the cerebral cortex, and there are significant differences in neuronal characteristics in different brain regions. The division of cortical brain regions in this study is not particularly accurate. Region1 includes the motor cortex and the prefrontal cortex. A recent work quantitatively investigated the whole brain input and output of CLA by using a large number of anterograde and retrograde viral tracing data and found that the prefrontal cortex module has more cell types projecting to the CLA than other cortex modules [35]. This may be the reason for the higher correlation between Region1 and CLA.

In the scheme of this paper, the rigidity and opacity of the silicon-based electrodes have a somewhat negative impact on the range of cortical calcium imaging. A recent study developed a flexible, insertable, and transparent microelectrode array (Neuro-FITM) to investigate the cortical–hippocampal coordination during hippocampal sharp-wave ripples [36]. This flexible electrode has almost no effect on the visual field range for cortical calcium imaging due to its better transparency, but its implantation depth range is limited. We have recently developed an ultra-thin flexible dual-mode microelectrode array [37], which can be combined with a wide-field microscope in the future to perform the simultaneous recording of electrophysiology and neurotransmitter

in the deep brain nuclei and large-scale cortical calcium imaging, at the same time eliminating the effect of rigid electrodes on the imaging range.

5. Conclusion

Here, we proposed a technical solution for synchronous recording of deep brain electrophysiology and wide-field cortical calcium imaging based on microelectrode arrays. We established a working mode of deep brain microelectrode array implantation and cortical chronic optical cranial window replacement and built a synchronous detection platform for electrophysiology and calcium imaging. We applied this strategy to the study of general anesthesia. Microelectrode arrays were implanted in the CLA to detect high-resolution neural electrophysiology information, while the skull was replaced with a chronic optical window to facilitate wide-field cortical calcium imaging. The mechanism of collaborative work between the CLA and the cortex was studied. This study achieved synchronous recording of the electrophysiological signals of CLA neurons and the calcium signals of the wide field cortical neurons in mouse throughout the entire process from wakefulness to anesthesia and then to wakefulness, and discovered their synchronous changes. This study summarized the electrophysiological characteristics of CLA neurons and the calcium signals characteristics of cortical neurons under different inhalation anesthesia concentrations. The synergistic effect between the microscopic neural action potential spike and macroscopic LFP in the CLA under high inhalation anesthesia concentrations was found, and the synchronization between cortical and CLA neurons was enhanced by deeper anesthesia. This study provides a new method and tool for synchronous detection of deep brain regions and cortex.

CRediT authorship contribution statement

Penghui Fan: Conceptualization, Methodology, Investigation, Validation, Writing – original draft. **Rujin Zhang:** Conceptualization, Methodology, Investigation, Validation, Writing – original draft. **Guihua Xiao:** Conceptualization, Methodology, Investigation, Validation, Writing – original draft. **Yilin Song:** Formal analysis, Writing – review & editing, Validation. **Chaowei Zhuang:** Methodology. **Lekang Yuan:** Formal analysis. **Fan Mo:** Methodology. **Botao Lu:** Methodology, Formal analysis. **Zhaojie Xu:** Formal analysis. **Yiding Wang:** Formal analysis. **Jinping Luo:** Investigation. **Mixia Wang:** Investigation. **Weidong Mi:** Investigation, Formal analysis. **Jiangbei Cao:** Conceptualization, Writing – review & editing. **Qionghai Dai:** Conceptualization, Writing – review & editing. **Xinxia Cai:** Conceptualization, Writing – review & editing, Funding acquisition.

Declaration of competing interest

The authors declare that they have no conflicts of interest in this work.

Acknowledgments

This work was sponsored by the National Natural Science Foundation of China (T2293730, T2293731, 62121003, 61960206012, 62333020 and 62171434), the National Key Research and Development Program of China (2022YFC2402501, 2022YFB3205602), Major Program of Scientific and Technical Innovation 2030 (2021ZD02016030).

Supplementary materials

Supplementary material associated with this article can be found, in the online version, at doi:10.1016/j.fmre.2023.12.012.

References

[1] B. Zhang, C. Deng, C. Ca, et al., In vivo neural interfaces—from small- to large-scale recording, Front. Nanotechnol. 4 (2022) 1–15.
[2] N. Chou, H. Shin, K. Kim, et al., A multimodal multi-shank fluorescence neural probe for cell-type-specific electrophysiology in multiple regions across a neural circuit, Adv. Sci. 9 (2022) 2103564.
[3] J. Xie, Y. Dai, Y. Xing, et al., PtNPs/rGO-GluOx/mPD directionally electroplated dual-mode microelectrode arrays for detecting the synergistic relationship between the cortex and hippocampus of epileptic rats, ACS Sensors 8 (2023) 1810–1818.
[4] B. Lu, P. Fan, M. Li, et al., Detection of neuronal defensive discharge information transmission and characteristics in periaqueductal gray double-subregions using PtNP/PEDOT:PSS modified microelectrode arrays, Microsystems Nanoeng 9 (2023) https://doi.org/10.1038/s41378-023-00546-8.
[5] E.T. Ahrens, J.W.M. Bulte, Tracking immune cells in vivo using magnetic resonance imaging, Nat. Rev. Immunol. 13 (2013) 755–763.
[6] C.K. Cook, Computed tomography of the brain: A pictorial review, Hosp. Med. 65 (2004) 8–12.
[7] P.K. Campbell, K.E. Jones, R.J. Huber, et al., A silicon-based, three-dimensional neural interface: Manufacturing processes for an intracortical electrode array, IEEE Trans. Biomed. Eng. 38 (1991) 758–768.
[8] R. Yuste, From the neuron doctrine to neural networks, Nat. Rev. Neurosci. 16 (2015) 487–497.
[9] D. Lee, H.C. Moon, B. Tran, et al., Characterization of tetrodes coated with Au nanoparticles (AuNPs) and PEDOT and their application to thalamic neural signal detection in vivo, Exp. Neurobiol. 27 (2018) 593–604.
[10] C.E. Schoonover, S.N. Ohashi, A.J.P. Fink, Representational drift in primary olfactory cortex, Nature 594 (2021) 541–546.
[11] T.D. Marks, M.J. Goard, Stimulus-dependent representational drift in primary visual cortex, Nat. Commun. 12 (2021) 5169.
[12] G. Buzsáki, C.A. Anastassiou, C. Koch, The origin of extracellular fields and currents — EEG, ECoG, LFP and spikes, Nat. Rev. Neurosci. 13 (2012) 407–420.
[13] Y. Son, H. Jenny Lee, J. Kim, et al., In vivo optical modulation of neural signals using monolithically integrated two-dimensional neural probe arrays, Sci. Rep. 5 (2015) 15466.
[14] J.P. Seymour, F. Wu, K.D. Wise, et al., State-of-the-art MEMS and microsystem tools for brain research, Microsystems Nanoeng. 3 (2017) 16066.
[15] S. Zhang, Y. Song, M. Wang, et al., A silicon based implantable microelectrode array for electrophysiological and dopamine recording from cortex to striatum in the non-human primate brain, Biosens. Bioelectron. 85 (2016) 53–61.
[16] E. He, S. Xu, G. Xiao, et al., MWCNTs/PEDOT:PSS nanocomposites-modified microelectrode array for spatial dynamics recording of epileptic discharges in multi-subregion of hippocampal slice, Sensors Actuators B Chem 329 (2021) 129190.
[17] R. Zhang, C. Zhuang, Z. Wang, et al., Simultaneous observation of mouse cortical and hippocampal neural dynamics under anesthesia through a cranial microprism window, Biosensors 12 (2022) 567.
[18] K. Narikiyo, R. Mizuguchi, A. Ajima, et al., The claustrum coordinates cortical slow-wave activity, Nat. Neurosci. 23 (2020) 741–753.
[19] I. Timofeev, S. Chauvette, Global control of sleep slow wave activity, Nat. Neurosci. 23 (2020) 693–695.
[20] M.Z. Koubeissi, F. Bartolomei, A. Beltagy, et al., Electrical stimulation of a small brain area reversibly disrupts consciousness, Epilepsy Behav 37 (2014) 32–35.
[21] T. Zhao, N. Wei, T. Li, et al., Transplantation of glutamatergic neuronal precursor cells in the paraventricular thalamus and claustrum facilitates awakening with recovery of consciousness, CNS Neurosci. Ther. (2023) https://doi.org/10.1111/cns.14137.
[22] C. Zhuang, J. Cao, R. Zhang, et al., Real-time brain-wide multi-planar microscopy for simultaneous cortex and hippocampus imaging at the cellular resolution in mice, Biomed. Opt. Express. 12 (2021) 1858.
[23] P. Fan, Y. Song, B. Lu, et al., PtNPs/PEDOT:PSS-modified microelectrode arrays reveal electrophysiological activities of different neurons in medial amygdala of mice under innate fear, Front. Neurosci. 16 (2022) 1–11.
[24] Y. Dai, Y. Song, J. Xie, et al., CB1-antibody modified liposomes for targeted modulation of epileptiform activities synchronously detected by microelectrode arrays, ACS Appl. Mater. Interfaces 12 (2020) 41148–41156.
[25] P.C. Vijn J.R., Sneyd, I.v. anaesthesia and EEG burst suppression in rats: Bolus injections and closed-loop infusions, Br. J. Anaesth. 81 (1998) 415–421.
[26] Y. Zhang, G. Zhang, X. Han, et al., Rapid detection of neurons in widefield calcium imaging datasets after training with synthetic data, Nat. Methods 20 (2023) 747–754.
[27] F. Amzica, What does burst suppression really mean? Epilepsy Behav. 49 (2015) 234–237.
[28] S. Gui, J. Li, M. Li, et al., Revealing the cortical glutamatergic neural activity during burst suppression by simultaneous wide field calcium imaging and electroencephalography in mice, Neuroscience 469 (2021) 110–124.
[29] K.B.J. Franklin, G. Paxinos, Paxinos and Franklin's the Mouse Brain in Stereotaxic Coordinates, Compact: The Coronal Plates and Diagrams, Academic press, 2019.
[30] Y. Qiang, P. Artoni, K.J. Seo, et al., Transparent arrays of bilayer-nanomesh microelectrodes for simultaneous electrophysiology and two-photon imaging in the brain, Sci. Adv. 4 (2018). https://doi.org/10.1126/sciadv.aat0626.
[31] B.P. Kerekes, K. Tóth, A. Kaszás, et al., Combined two-photon imaging, electrophysiological, and anatomical investigation of the human neocortex in vitro, Neurophotonics 1 (2014) 011013.
[32] Y. Bando, M. Wenzel, R. Yuste, Simultaneous two-photon imaging of action potentials and subthreshold inputs in vivo, Nat. Commun. 12 (2021) 1–12.

[33] E.G. McBride, S.R. Gandhi, J.R. Kuyat, et al., Influence of claustrum on cortex varies by area, layer, and cell type, Neuron 111 (2023) 275–290.
[34] J. Jackson, J.B. Smith, A.K. Lee, The anatomy and physiology of claustrum-cortex interactions, Annu. Rev. Neurosci. 43 (2020) 231–247.
[35] Q. Wang, Y. Wang, H.-C. Kuo, et al., Regional and cell-type-specific afferent and efferent projections of the mouse claustrum, Cell Rep 42 (2023) 112118.
[36] X. Liu, C. Ren, Y. Lu, et al., Multimodal neural recordings with Neuro-FITM uncover diverse patterns of cortical–hippocampal interactions, Nat. Neurosci. 24 (2021) 886–896.
[37] P. Fan, Y. Wang, Y. Dai, et al., Flexible microelectrode array probe for simultaneous detection of neural discharge and dopamine in striatum of mice aversion system, Sensors Actuators B Chem. 390 (2023) 133990.

Author profile

Penghui Fan received B.E. degree in electronic science and technology in 2018 from University of Electronic Science and Technology of China. He received his Ph.D degree in State Key Laboratory of Transducer Technology, Aerospace Information Research Institute, Chinese Academy of Sciences. His research interests include microelectrode fabrication and electrophysiological and electrochemical detection.

Jiangbei Cao is the deputy director, chief physician, professor, and doctoral supervisor of the Anesthesia and Surgery Center of the First Medical Center of PLA General Hospital. He has published 23 SCI papers and 54 Chinese papers. He has received 6 patents. His main research interests include the protection of perioperative organ function, especially the regulation and protection of central nervous system function.

Qionghai Dai is a professor at Tsinghua University. His research interests include brain imaging and intelligent technology. He made important contributions to the field of computational imaging, especially in the field of computational microscopy. He published more than 500 articles and applied for more than 500 patents.

Xinxia Cai received her PhD degree in bioelectronics, electronics & electrical engineering from Glasgow University in UK. She is distinguished professor of the Aerospace Information Research Institute of the Chinese Academy of Sciences, winner of the National Science Fund for Distinguished Young Scholars, academic leader of the Micro-nano Sensing Technology Innovation Research Group of National Natural Science Foundation of China (NSFC). Prof. Cai mainly focuses on micro-nano biosensors and microsystems such as brain-computer interface neural microelectrode arrays for a long time, and is the research leader of the major project of the Interdisciplinary Department of NSFC.